Journal of
Composites Science

MDPI

Article

Plasma-Enhanced Alginate Pre-Treatment of Short Flax Fibers for Improved Thermo-Mechanical Properties of PLA Composites

Ghane Moradkhani [1,2,3,4], Jacopo Profili [4], Alex Destrieux [4], Mathieu Robert [1,2,3], Gaétan Laroche [3,4], Saïd Elkoun [1,2,3,*], Frej Mighri [2,5] and Pascal Y. Vuillaume [2,6]

1 Center for Innovation in Technological Eco-Design (CITE), University of Sherbrooke, Sherbrooke, QC J1K 2R1, Canada
2 Research Center for High Performance Polymer and Composite Systems, CREPEC, Montreal, QC H3A 0C3, Canada
3 Quebec Center for Advanced Materials, QCAM, Monteal, QC H2V 0B3, Canada
4 Centre de Recherche du Centre Hospitalier Universitaire de Québec, Hôpital St-François d'Assise, Québec City, QC G1L 3L5, Canada; alex.destrieux1@ulaval.ca (A.D.)
5 Department of Chemical Engineering, Laval University, Quebec City, QC G1V 0A6, Canada
6 Coalia, Thetford Mines, QC G6G 1N1, Canada
* Correspondence: said.elkoun@usherbrooke.ca

Abstract: This research centered on enhancing the mechanical properties of sustainable composite materials made from short flax fibers. Challenges associated with fiber–matrix adhesion and moisture absorption were systematically addressed. A water–alginate pre-treatment, combined with plasma modification, was employed to stabilize the fibers, ensuring their optimal preparation and improved compatibility with biopolymers. A thorough investigation of the effect of the plasma modulation using a duty cycle (DC) was conducted, and extensive physicochemical and mechanical analyses were performed. These efforts revealed conditions that preserved fiber integrity while significantly improving surface characteristics. Techniques such as optical emission spectroscopy (OES), Fourier transform infrared spectroscopy (FTIR), differential scanning calorimetry (DSC), and Dynamic Mechanical Analysis (DMA) were utilized, providing a comprehensive understanding of the transformations induced by the plasma treatment. The findings underscored the critical role of alginate and precise plasma settings in enhancing the mechanical properties of the composites. Ultimately, this study made a substantial contribution to the field of eco-friendly materials, showcasing the potential of short flax fibers in sustainable composite applications and setting the stage for future advancements in this area.

Keywords: short flax fiber; sodium alginate; DBD; mechanical properties

Citation: Moradkhani, G.; Profili, J.; Destrieux, A.; Robert, M.; Laroche, G.; Elkoun, S.; Mighri, F.; Vuillaume, P.Y. Plasma-Enhanced Alginate Pre-Treatment of Short Flax Fibers for Improved Thermo-Mechanical Properties of PLA Composites. *J. Compos. Sci.* **2024**, *8*, 106. https://doi.org/10.3390/jcs8030106

Academic Editors: Francesco Tornabene, Mohamed Ragoubi, Frédéric Becquart and Ahmed Koubaa

Received: 21 January 2024
Revised: 26 February 2024
Accepted: 14 March 2024
Published: 18 March 2024

1. Introduction

Natural fibers are gaining recognition for their role in eco-friendly composite materials [1]. With renewable, biodegradable properties and strong mechanical attributes, they are ideal for reinforcing polymer matrices. The natural fiber composite market, valued at USD 328 million in 2023, is projected to reach USD 424 million by 2028 [2]. This growth is mostly driven by the rising demand for sustainability from the automotive and construction industries along with a growing understanding of additional benefits of natural fibers over the synthetic ones [3,4]. Among these natural fibers, short flax fibers have emerged as particularly promising materials due to their high tensile strength, making them ideal for load-bearing components. Additionally, their stiffness and rigidity make them excellent reinforcements in composite materials [5,6]. However, a critical challenge is assuring a strong bond with polymer matrices, all while effectively handling moisture absorption [7,8]. This dual concern is essential for preserving the mechanical integrity of flax fiber composites over time [9]. Over two decades of dedicated research, scientists have

worked to address this adhesion challenge, leading to substantial advancements in both mechanical performance and the refinement of surface characteristics, such as adhesion strength and surface texture [10–12].

Today, natural fibers can be modified either by altering the fiber surface or partially changing the chemical structure. For composites, surface treatment methods are employed to enhance intermolecular bonding with the matrix phase. However, chemical modifications have significant drawbacks, requiring large volumes of chemicals and extended processing times [13]. Recently, plasma modification has gained popularity as a more environmentally sustainable and time-saving option, offering a quick and eco-friendly approach to surface modification [14–16]. Plasma-induced changes in the physicochemical and microstructural properties of natural fibers lead to enhanced adhesion in composites [17,18].

It is also interesting to note that there is also a surge in exploring eco-friendly ways to blend natural materials like lignin, tannins, proteins, and oils with biobased binders [19,20]. A standout example is the success of condensed tannins in binding non-woven natural fibers, wood particleboards, and materials like flax or hemp [21,22]. Bayart et al. [23] introduced waste-derived lignin and tannin to boost the adhesion in flax fiber-reinforced composites, aiming for truly sustainable materials. They achieved remarkable results with just a 1% coating of tannin or lignin, especially with tannin, which showed a strong affinity with PLA and flax fibers. However, using higher amounts of these compounds led to thicker coatings and some issues with homogeneity, affecting the overall strength of the material. It is worth noting that the expensive extraction process of tannins, along with the high-water usage, currently limit their widespread use in industries [24]. In this context, alginate, sourced from marine biomass could be considered a viable alternative. This product is a valuable natural polysaccharide widely applied across industries, including food and textiles [25,26], where it serves as a gelling-agent, stabilizer, and thickener [27]. John et al. [28]. introduced flax fibers as a natural reinforcement within PLA and PHBV composites. These fibers were chemically modified using a dip-coating method with 2% and 4% sodium alginate solutions. This treatment was employed to enhance the compatibility of the fibers with the biopolymers. The integration of these modified fibers aimed to create a more robust and sustainable material compared to using biopolymers alone. The study's findings indicated that treating flax fibers with alginate led to a notable enhancement in the strength and heat resistance of the resulting composites.

In this research, a comprehensive solution was identified to tackle the challenges associated with plasma treatment in the incorporation of short flax fibers into layered composites. The fibers were stabilized and prepared for effective plasma exposure through the application of a water–alginate pre-treatment. An in-depth examination of various plasma duty cycles (DCs) was conducted to identify the optimal conditions for the integrity of the fibers while enhancing their surface properties. Additional analyses were conducted on both the plasma process as well as the composites to provide a clear and comprehensive understanding of the chemical and mechanical transformations induced after the plasma treatment.

2. Experiment

2.1. Materials

The short flax fibers employed in this study were sourced from Fibers Recherches Développement (FRD) in France, ensuring a high standard of quality. The average diameter of these fibers was meticulously measured to be approximately 0.22 mm through optical microscopy. Additionally, the average fiber length covered from 20 to 50 mm, offering a versatile selection for experimentation. The samples selected for plasma treatment have dimensions of 6×4 cm^2. The PLA 4032D pellets were supplied by Natureworks, Plymouth, MN, USA. In order to improve the adherence and stability of the fibers, sodium alginate derived from brown algae was utilized, which was procured from supplier Sigma Aldrich, Oakville, Canada.

2.2. Treatment of Flax Fibers

2.2.1. Preparation of Flax Fiber with Sodium Alginate

The process began with a measurement of 0.5 g of sodium alginate, which was gently mixed with 100 mL of deionized water. Simultaneously, 1.5 g of short flax fiber was placed in a Petri dish. Once in position, 30 g of the alginate solution was gently poured over the fibers. To ensure an even distribution and consolidation, a clamp was applied, securing the fibers to a mesh-covered Petri dish, which was layered with a film of Teflon. The carefully assembled arrangement was then transferred to an oven, where it was subjected to a controlled environment at 60 degrees Celsius. After 6 h, the clamp was thoughtfully removed to prevent any unwanted adhesion. Subsequently, the treated flax fibers were returned to the oven, where they underwent an additional 24 h curing process.

2.2.2. Plasma Pre-Treatment of Modified Flax Fiber

In the pre-treatment process of the flax mat, a specific configuration was employed, utilizing a dielectric barrier discharge (DBD) reactor equipped with parallel plate electrodes. The experimental setup consisted of positioning a sample measuring 5.0 $\times$ 3.0 cm^2 on the ground electrode. The dimensions of the electrodes used were 6.0 $\times$ 4.0 cm^2, with a thickness of 0.64 mm. To initiate the discharge, an arbitrary function generator (AFG-2021, Tektronix, Beaverton, OR, USA) was connected to an audio amplifier PL380 from QSC Audio Products, LLC (Costa Mesa, CA, USA). The system was operated within a frequency range spanning from 10 Hz to 100 kHz. In this study, a transformer manufactured by Raftabtronics located in Longwood, FL, USA was used to generate the high voltage. This transformer allowed us to reach a maximum peak-to-peak voltage of 18 kV_{pp} (ratio 11,500) while operating within a frequency range of 5 to 15 kHz. The voltage supplied at the transformer's exit was measured using a high-voltage probe (P6015A, with a 1000$\times$ attenuation, manufactured by Tektronix). Additionally, a N_2 gas flow rate of 10 SLM (Standard Liters per Minute) was maintained while keeping a constant 1 mm gap between the electrodes. To control the power, the discharge was modulated using a DC. Different DCs of 10%, 30%, 50%, and 100% were experimented with. This adjustment involved modifying the sinusoidal signal with a squared waveform, which is shown in Figure 1. The voltage applied during the experiments typically ranged from 15 to 16 kV, with a fixed frequency of 10 kHz. In addition, temperature changes during the experiments were monitored using an infrared thermometer (Klein Tools). Temperature measurements were taken every minute for a duration of five minutes to ensure the precise monitoring of the dielectric temperature.

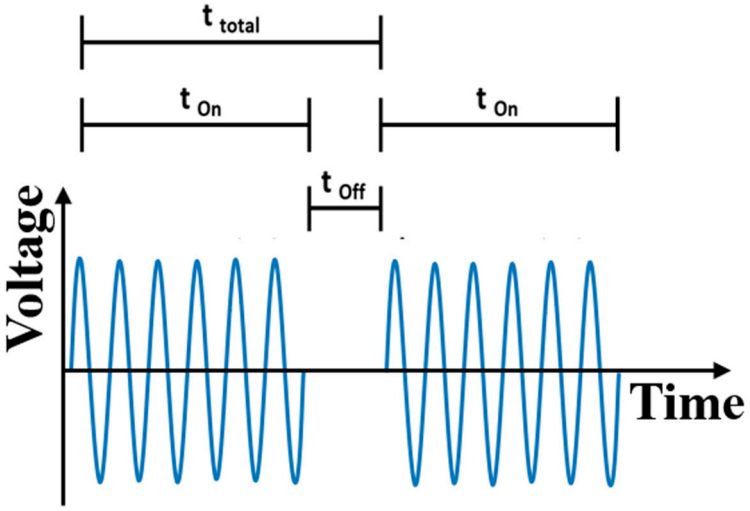

Figure 1. Pulse Width Modulation (PWM) waveform: 't_{total}' indicates the complete cycle duration; 't_{On}', the duration of the high-voltage pulse; and 't_{Off}', the low- or zero-voltage interval, illustrating the duty cycle of an electrical signal over time.

2.3. Composite Processing

To create the composite, six layers of PLA were combined with five layers of specially treated flax matting. This process resulted in a composite material that synergistically integrated the favorable characteristics of both PLA and the treated flax mats. For optimal bonding, the composite underwent a controlled thermal (180 °C) and mechanical (44 MPa) shaping process during five minutes. This facilitated a strong and enduring connection between the PLA and the treated flax mats, ultimately producing a composite material distinguished by heightened strength and enhanced performance.

2.4. Characterization Methods

2.4.1. OES

The emission spectra were recorded using an HR4000CG-UV-NIR spectrometer (OceanOptics, Orlando, FL, USA). Light was collected through a 5 μm slit, directed toward a lens for collimation, and then passed through a diffraction grating (HC-1, 300 lines/mm). Following wavelength separation, the light was directed to a focusing mirror and subsequently to a CCD detector (Toshiba TCD1304AP linear CCD array, 3648 pixels, 100 photons per count at 800 nm). The spectrometer operates in the ultraviolet, visible, and near-infrared ranges (200 nm–1100 nm), with an optical resolution of 0.75 nm at full width at half maximum (FWHM). Due to the non-flatness of the fiber, the discharge was not ignited homogeneously over the electrode area. Therefore, the optical fiber used to record the spectra was aligned to a region where the discharge was properly ignited, though its position varied from one sample to another. For the 10% DC condition, the intensity was very low, and the discharge did not ignite over the entire surface of the electrodes. The acquisition time was thus set to 10 s, and only one spectrum was taken. For the other conditions (30%, 50%, and 100% DC), the integration time was set to 1 s, and each spectrum was an average of 5 scans. For all conditions, one spectrum was recorded every minute for a duration of 5 min.

2.4.2. FTIR

The fiber composition and structure were analyzed using a Cary 660 FTIR spectrophotometer, provided by Agilent Technologies. This device was equipped with a deuterated triglycine sulfate (DTGS) detector from Harrick Scientific Products and a silicon-based attenuated total reflectance (ATR) attachment. A total of 128 scans were conducted for each sample to ensure homogeneity in the data, with the spectral resolution set at 4 cm^{-1}. Measurements were taken at three distinct points on each layer, aiming for consistency and reliability in the results. Additionally, the internal reflection element (IRE) used in the setup had a refractive index of 2.41, while the flax fibers, serving as the substrate, had a refractive index of 1.59. The infrared beam was consistently directed at the sample at an angle of 45°.

2.4.3. XPS

The outer layer of the flax fibers was examined using a PHI 5600-ci spectrometer, located at Physical Electronics in Chanhassen, Minnesota, USA. The procedure was conducted in a high-vacuum environment of 8×10^{-9} Torr, involving the detection of photoelectrons at a 45° angle. To counteract the effects of surface charging, the binding energy peak of aliphatic carbon (C-C/C-H) was calibrated to 285.0 eV. Each of the samples analyzed during this study covered an area of approximately 0.05 mm^2. Following background correction using Shirley-type subtraction, the C1s envelopes were subjected to thorough analysis. This analysis was performed using Gaussian–Lorentzian functions and facilitated by Casa XPS software, version 2.3.16. Notably, the recorded FWHM values fell within the range of 0.7 to 1.5, ensuring a high level of precision in the obtained data. To ascertain the chemical consistency of the treatments, three separate analyses were conducted on each sample, allowing for the calculation of mean values and standard deviations.

2.4.4. SEM

The surface morphology of the flax fibers was meticulously examined using a Quanta250 Scanning Electron Microscope (SEM), manufactured by Thermo Fisher Scientific, Hillsboro, OR, USA. This instrument can deliver high-resolution images, and for the purposes of this study, it was operated at a voltage of 1 kV to achieve a resolution of 1.4 nanometers. Considering the low conductivity of the flax fiber substrates, a conductive coating was deposited prior to analysis. This was achieved by evenly depositing a thin layer of gold–palladium (Au-Pd) onto the surface of each sample. The coating served dual purposes: it facilitated charge dissipation during imaging, and it enhanced the overall quality of the images acquired.

2.4.5. DSC

Differential scanning calorimetry (DSC) measurements were carried out under a nitrogen atmosphere using a Q200 instrument from TA Instruments. The samples selected for these experiments had weights ranging between 7 and 10 milligrams, ensuring a consistent basis for analysis. The thermal behaviors of the materials were examined across a temperature range of 0 °C to 220 °C. The DSC profiles were captured through three distinct phases: an initial heating period, a subsequent cooling phase, and a final reheating stage, with the temperature being raised at a constant rate of 10 °C per minute. To mitigate any potential effects from the prior thermal exposure of the samples, the analysis primarily relied on data gathered during the second heating phase. This approach was taken to ensure that the results accurately and reliably reflected the true thermal properties of the materials.

2.4.6. DMA

The mechanical properties of the composite material were rigorously investigated using Dynamic Mechanical Analysis (DMA), employing a Q850 DMA instrument from TA Instruments Ltd., Eden Prairie, MN, USA. The goal of this analysis was to elucidate how the material's behavior changes with temperature. The procedure entailed a gradual increase in temperature from −20 °C to 140 °C, with a constant heating rate of 3 °C per minute maintained throughout the experiment. Additionally, the frequency was held steady at 1 Hz to ensure consistent testing conditions. For the evaluation of the material's mechanical characteristics, the single cantilever bending method was utilized, applied to samples meticulously prepared to precise dimensions of $2 \times 12 \times 17.5$ mm^3.

3. Results and Discussion

3.1. OES

During the pre-treatment of the flax fibers, optical emission spectroscopy (OES) was used to collect data on the discharge over time. Figure 2 presents a typical nitrogen discharge spectrum in the presence of the fibers, showcasing several notable features. The main peaks correspond to the second positive system (SPS) of nitrogen, arising from photon emission during the de-excitation of nitrogen from the $C^3\Pi_u$ excited state to the lower $B^3\Pi_g$ level. One must consider that peaks of the N_2 SPS are always present in nitrogen discharges generated at atmospheric pressure [29]. Note that all the spectra are normalized to the 337.13 nm emission of N_2 ($\nu' = 0 \rightarrow v'' = 0$). Also, the different peaks in the spectrum correspond to various vibrational transitions between the upper and lower electronic states, leading to distinct $\Delta\nu$ regions (highlighted in red for nitrogen). Additionally, the presence of two other molecular species in the gas phase was observed. At lower wavelengths, emissions from NO are visible, corresponding to the $A^2\Sigma^+ \rightarrow X^2\Pi_r$ transition (γ system), with the observed transitions exhibiting a vibrational number difference of $\Delta\nu = -1$. NO emissions were frequently observed in the N_2 plasma when oxygen was admixed [30].The treatment of the fibers also revealed emissions from the CN radical, corresponding to the electronic transition $B^2\Sigma^+ \rightarrow X^2\Sigma^+$. Two vibrational sequences, $\Delta\nu = 0$ and $\Delta\nu = -1$,

were observed for CN. Notably, there was a rise in CN intensity over time, as illustrated in the inset of Figure 2.

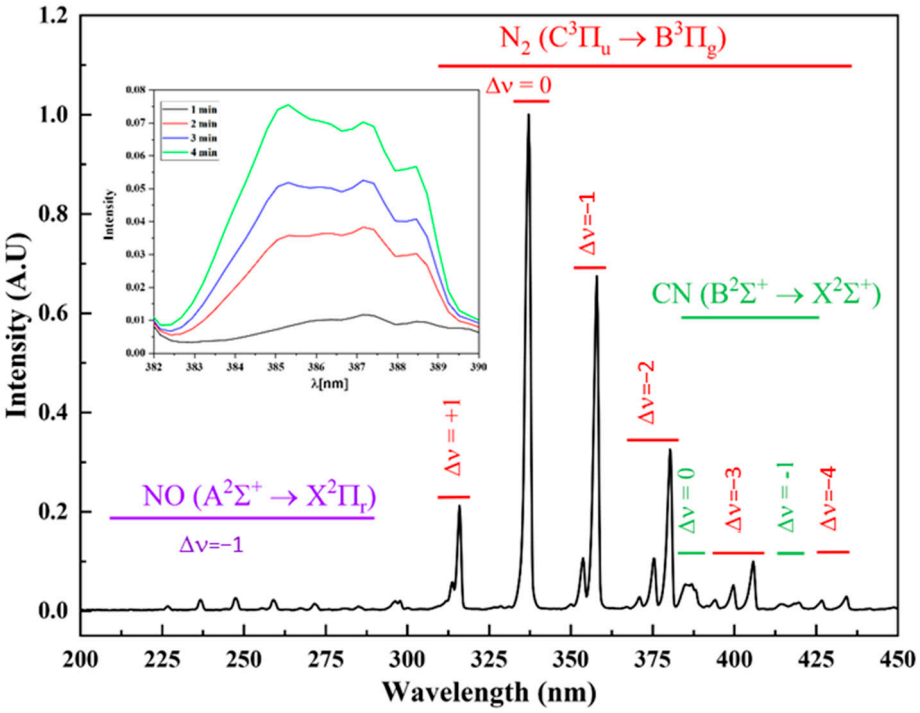

Figure 2. Typical spectrum obtained in nitrogen discharge during the treatment of flax fibers. The spectrum was obtained at 50% DC, 15 kVpp, 10 kHz, after 4 min of discharge. The inset is a zoom in on the CN; Δν = 0 emission region for different times.

To delve deeper into these variations, they are plotted over time for the four DCs, alongside the dielectric temperature, in Figure 3a. Across all DCs, an increase in CN intensity is observed over time. Furthermore, higher DCs correspond to higher emission intensities. In terms of the temperature measured on the dielectric (high voltage side), the conditions can be grouped into two categories. For the 10% and 30% DCs, the temperature rise is modest ($\Delta T < 10$ K), while for the 50% and 100% DCs, there is a more substantial increase in temperature, with $\Delta T_{50\%} = 34$ K and $\Delta T_{100\%} = 64$ K. This temperature rise is primarily attributed to longer plasma ignition times under these conditions. One must consider that in this range of temperature, a possible degradation of the fibers at 50% and 100% DCs could be observed. In this sense, CN emissions have previously been observed for polymers treated in different dielectric barrier discharge setups, often attributed to the etching of carbon from the polymers [31,32]. A similar phenomenon might be occurring here, potentially enhanced at higher temperatures where the fibers degrade, leading to the release of C atoms into the discharge and their subsequent recombination with nitrogen to form CN. Figure 3b presents the variation in NO emissions for each DC, alongside the vibrational temperature (T_{vib}) calculated from the Boltzmann plot of the N_2 (C-B, $\Delta\nu = -2$) sequence [33]. For both parameters, no clear trend over time was observed; thus, only the mean value and standard deviation are shown. Due to very low emissions and long integration times for NO, its intensity cannot be reliably distinguished from the noise, and is therefore not presented. In examining the NO emissions, a decrease is noted from the 30% DC to the 100% DC, with the 50% DC exhibiting a strong standard deviation. This deviation is attributed to a gradual temperature rise, similar to that observed at the 10% and 30% DCs during the initial 2 min. Over the 5 min period, NO emissions decrease from 0.045 A.U. (close to 30%) to 0.022 A.U. (close to 100%). However, examining the vibrational temperature reveals two distinct trends. For the 10% and 30% DCs, T_{vib} ranges between 2250 K and 2300 K, dropping to around 2150 K when the DC increases to 50% or 100%. This

change could indicate a shift in discharge chemistry, potentially related to fiber degradation, a topic that will be explored in subsequent sections.

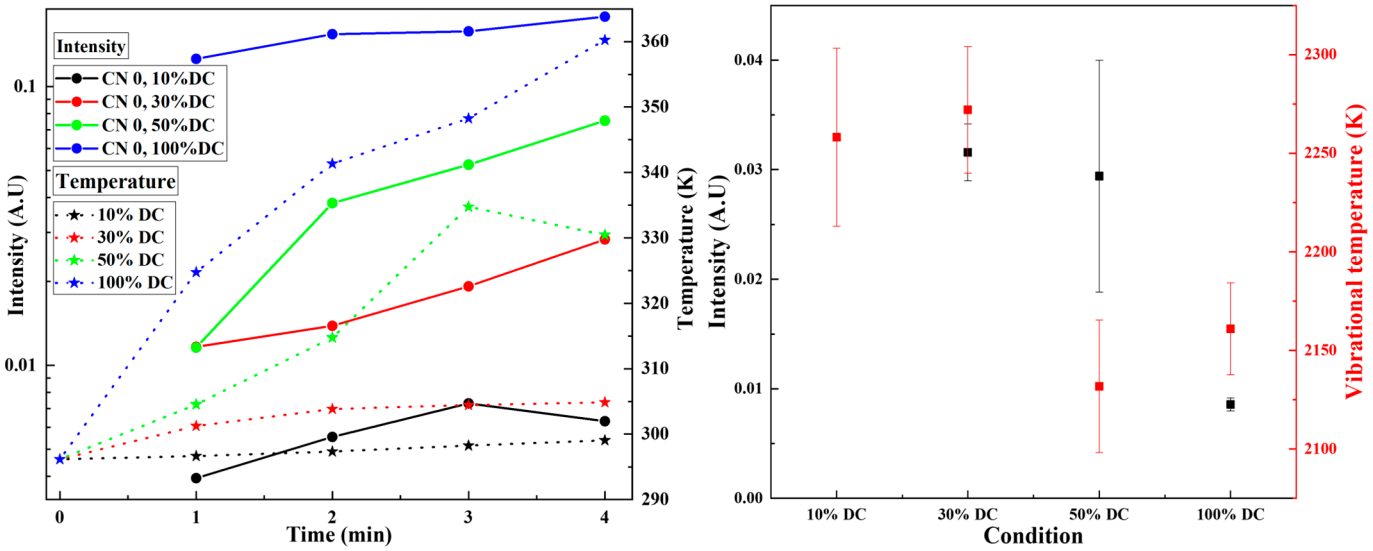

Figure 3. (**a**) Intensity variation in the CN emissions along with the dielectric temperature and (**b**) intensity variation in the NO emissions along with the vibrational temperature (black and red squares stand for intensity and vibrational temperature respectively).

3.2. FTIR of Non-Treated and Treated Samples

Figure 4 offers a detailed view of the ATR-FTIR spectra for untreated flax fiber and sodium alginate, each spectrum revealing the unique chemical compositions of these two natural polymers derived from plant and seaweed origins, respectively. In the spectrum of flax fiber, we observe a prominent peak centered at 3344 cm^{-1}, which is characteristic of hydroxyl (OH) stretching vibrations. This feature is a strong indicator of the presence of H_2O and hydroxyl groups, which are abundant in plant cell materials. Moreover, the CH_2 stretching vibrations, evident at 2915 cm^{-1} and 2850 cm^{-1}, suggest the presence of aliphatic structures, which could be related to the pectins or waxes found in the fiber. The peak at 1640 cm^{-1} aligns with the vibrations of water molecules, further supporting the presence of absorbed moisture in the cellulose structure. The spectrum of flax fiber also unveils additional bands that are indicative of its complex structure, including lignin, microcrystalline cellulose, polysaccharides, and the distinctive β-glycosidic linkages that are typical of cellulose. For a more detailed exploration of these spectral features, readers are referred to our previous work [18]. Comparative ATR-FTIR spectral band assignments are listed in Table 1.

The sodium alginate spectrum, while sharing some spectral features with that of flax fiber due to their polysaccharidic nature, also presents unique bands that highlight its marine origin. The OH stretching vibration at 3344 cm^{-1} as well as the CH_2 groups at 2915 cm^{-1} and 2850 cm^{-1} are present, demonstrating structural similarities between the two. The hydration of sodium alginate is confirmed by the band at 1646 cm^{-1}, resonating with water molecule vibrations [34]. A notable band around 1108 cm^{-1} underscores the polysaccharidic backbone of sodium alginate. Furthermore, the spectrum of sodium alginate exhibits bands at 1596 cm^{-1} and 1409 cm^{-1}, which are indicative of the asymmetric and symmetric stretching of COO- groups, respectively. These are a consequence of the ionic bonds formed with sodium ions. Distinct peaks at 950 cm^{-1}, 888 cm^{-1}, and 817 cm^{-1} reveal the presence of guluronic and mannuronic acids, the fundamental constituents of alginate, giving it a unique spectral signature that distinguishes it from other polysaccharides [35,36].

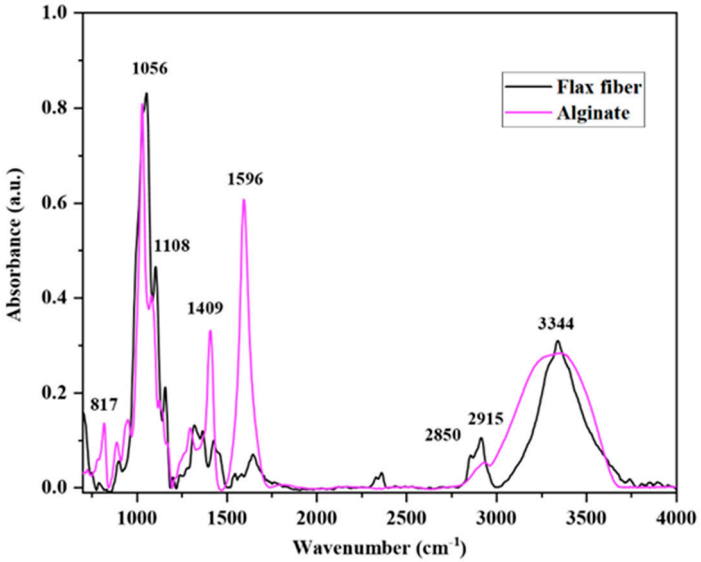

Figure 4. FTIR spectra of flax fiber and sodium alginate, highlighting key functional group vibrations.

Table 1. Comparative ATR-FTIR spectral band assignments for untreated flax fiber and sodium alginate.

Wavenumber (cm^{-1})	Flax Fiber Attribution	Sodium Alginate Attribution
3344	Hydroxyl (OH) stretching vibrations	Hydroxyl (OH) stretching vibrations
2915	CH_2 asymmetrical stretching	CH_2 asymmetrical stretching
2850	CH_2 symmetrical stretching	CH_2 symmetrical stretching
1646	Water molecule vibrational mode	Water molecule vibrational mode
1596		Asymmetric stretching of COO- groups
1432	C–H_3 asymmetric deformation in lignin	
1409		Symmetric stretching of COO- groups
1370	Microcrystalline cellulose vibrations	
1335	Microcrystalline cellulose vibrations	
1315	Microcrystalline cellulose vibrations	
1270	C-O stretching in ester groups	
1160	Polysaccharides in cellulose (ring breathing)	
1108	Glycosidic ether band	Glycosidic ether band
1056	C-O-C pyranose ring skeletal vibrations	
1033	C-O-C pyranose ring skeletal vibrations	
950		Guluronic acids in sodium alginate
900	β-glycosidic linkages in cellulose	
888		Mannuronic acids in sodium alginate
817		Mannuronic acids in sodium alginate

In the study of flax–alginate composites treated with plasma, shown in Figure 5, clear changes in the spectra were seen. The samples treated with 10% and 30% plasma showed different peaks in the CH region, especially around 2856 cm^{-1} and 2924 cm^{-1}. These peaks are linked to the stretching of CH_2 groups and suggest that the treatment may have caused changes in the molecular structure. The combination of sodium alginate and plasma treatment could have added new groups to the molecules or made existing ones more effective. These changes might help the fibers stick better to the alginate material.

In the sample treated at 30% DC, a peak at 1713 cm^{-1} was observed, typically associated with the stretching of C=O groups found in carbonyl. This suggests that the plasma treatment may have induced oxidation, introducing polar groups onto the material's surface [37,38]. For the flax–alginate sample treated with 50% DC, the peak suggesting oxidation was also present but smaller and less intense, indicating a slight change. Accordingly to the literature, such changes could increase surface energy and enhance the adhesion properties with the PLA matrix [39]. In contrast, the sample with a 100% DC (i.e.,

no modulation) plasma treatment showed a shift in the carbonyl peak from 1730 cm^{-1} to 1697 cm^{-1} suggesting an alteration in the electron density around the carbonyl groups, which is indicative of molecular restructuring or new interactions [40]. Similarly, the peak around 1600 cm^{-1} also shifted to a lower wavenumber, which could reflect changes in the hydrogen bonding network within the cellulose—a primary component of flax fibers.

To sum up, plasma treatment has changed the chemical makeup of the flax–alginate samples. The changes in the sample with 30% plasma are especially interesting and could be important for future analysis.

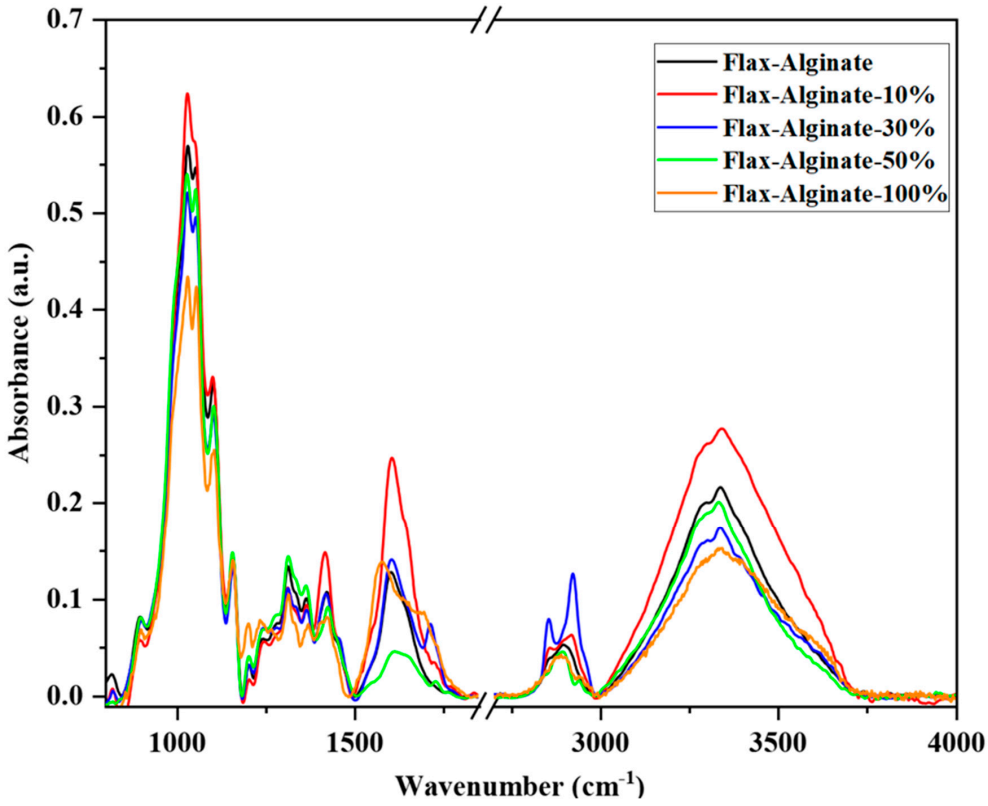

Figure 5. FTIR spectral overlay for flax–alginate composites, each line corresponding to a single plasma treatment intensity. The regions with higher modifications induced by plasma are highlighted in the region between 800–1750 and 2750–4000.

3.3. XPS

XPS analysis was conducted to understand the surface chemical composition of untreated and treated flax fiber substrates. As presented in Table 2, the untreated flax fiber primarily consisted of carbon (75.5%) and oxygen (24.5%), without any detectable amounts of nitrogen or sodium. Upon introducing sodium alginate to the substrate, a decrease in carbon content to 71.5% was observed, while the oxygen content slightly increased to 27.1%. This suggests that the alginate's incorporation introduces more oxygen-rich functional groups to the surface. Additionally, the presence of sodium at 1.42% is a direct indication of the sodium alginate's contribution. For the plasma-treated samples, some changes were noticed. The 10% and 30% plasma treatments resulted in reduced carbon levels to around 64% and an increase in oxygen content to roughly 33.7% for the 10% plasma sample. The introduction of nitrogen in these samples, especially noticeable in the 10% plasma treatment, may be due to the plasma process facilitating the formation or exposure of nitrogen-containing functional groups or introduction from N atoms coming from the discharge. The 100% plasma-treated sample showed a carbon content of 62.4% and an oxygen level of 34%. The notably higher sodium content of 2.98% in this sample

might suggest a more pronounced interaction or exposure of sodium alginate on the surface due to the intense plasma treatment.

Table 2. Elemental compositions and atomic ratios of untreated and treated flax fiber substrates determined via XPS.

Sample Name	C	O	N	Na	O/C
Flax fiber	75.5 ± 0.84	24.5 ± 0.84	-	-	0.3245
Sodium alginate	65.9 ± 1.53	28.1 ± 1.70	2.26 ± 0.17	3.83 ± 0.45	0.4264
Flax–Alginate	71.5 ± 3.60	27.1 ± 3.23	-	1.42 ± 0.60	0.3790
Flax–Alginate 10%	64.1 ± 1.84	33.7 ± 1.67	0.95 ± 0.25	1.25 ± 0.47	0.5257
Flax–Alginate 30%	64.2 ± 0.23	33.6 ± 0.17	0.78 ± 0.18	1.43 ± 0.11	0.5234
Flax–Alginate 50%	59.2 ± 1.65	38.5 ± 1.53	0.88 ± 0.25	1.42 ± 0.15	0.6503
Flax–Alginate 100%	62.4 ± 0.25	34.0 ± 0.17	0.63 ± 0.04	2.98 ± 0.10	0.5449

The XPS spectra of untreated flax fiber and sodium alginate samples, presented in Figure 6, provide a detailed analysis of the surface chemistry of these materials. The C1s spectrum of the untreated flax fiber reveals several prominent peaks that warrant further investigation. The peak at approximately 284.8 eV, attributed to C−C (sp^3) bonding, encompasses both the aromatic structures found in lignin and the aliphatic carbons in cellulose, hemicelluloses, and waxes. At around 286.3 eV, the C−O bonds were detected, which is indicative of hydroxyl groups in cellulose and ether bonds in lignin, among other oxygenated compounds. The carbonyl group, denoted by C=O, appears near 287.6 eV, a feature commonly associated with cellulose [41]. Furthermore, evidence of ester or carboxylic functionalities was observed at approximately 288.8 eV [42,43]. When examining the C1s spectra of sodium alginate, one can observe a peak around 284.8 eV. The significant peak at 286.3 eV denotes the presence of C−O bonds, which highlight the ether linkages within the polymer. Additionally, the resonance at 287.6 eV in the XPS spectrum provides valuable insights into the carboxylate groups present in sodium alginate. It is also plausible that the signal observed at around 288.8 eV could be attributed to residual carboxylic acid groups or other esterified structures [44]. A distinctive peak at approximately 290.2 eV in the C1s spectrum, labeled as the 'C5 Carbon Peak,' indicates an unusual carbon environment not typically seen in sodium alginate structures. Tam et al. [45] have associated such peaks with atmospheric CO_2 adsorption on sample surfaces, leading to potential carbonate species formation. This phenomenon could account for the observed peak, aside from any impurities or sample additives. Based on the data in Table 2, flax fiber, with an O/C ratio of 0.32, has fewer oxygen-containing groups on its surface, making it less hydrophilic than sodium alginate. Sodium alginate has a higher O/C ratio of 0.4264, which means it has more oxygen-containing groups, contributing to its more hydrophilic surface and a more varied array of carbon–oxygen bonds, as shown in Figure 6.

The high-resolution XPS spectra presented in Figure 7 reveal distinct chemical changes in the flax–alginate composites following plasma treatment, with a notable change in the C−O bond peak at 286.3 eV for all treated samples. This suggests an enhancement of oxygen-containing functional groups on the sample surfaces. It is confirmed in Table 2 that the O/C ratio for the composites rises from 0.37 to 0.52 and 0.52 after the 10% and 30% plasma treatments, respectively. This trend is consistent with the findings of Bozaci et al., who also reported similar changes in the O/C ratio following plasma treatment [10]. Moreover, the flax–alginate 50% DC composite shows a marked increase in this peak, indicating that carbon is preferentially removed from the surface due to its lower binding energy compared to oxygen, which could temporarily increase the O/C ratio on the surface [46]. Conversely, the flax–alginate 100% DC sample experiences a more substantial increase in the C1s peak, which may be attributed to a degradation as suggested in the OES section. This degradation could be related to the conversion of carbon into CO_2, leading to a significant decrease in the O/C ratio [47]. Additionally, a trend at 287.6 eV, associated with the C=O bond, suggests the presence or enhancement of carbonyl groups. Also, in the

FTIR analysis, these peaks were confirmed, and for flax–alginate 30%, it was more intense. The plasma treatment might have facilitated reactions that lead to higher concentrations of these groups. Furthermore, a distinct peak around 288.8 eV in the treated samples indicates potential plasma-induced oxidation or cross-linking reactions, emphasizing the presence of functional groups such as esters or carboxylic acids. In summary, plasma treatment has introduced notable chemical modifications to the surface of the flax–alginate composite.

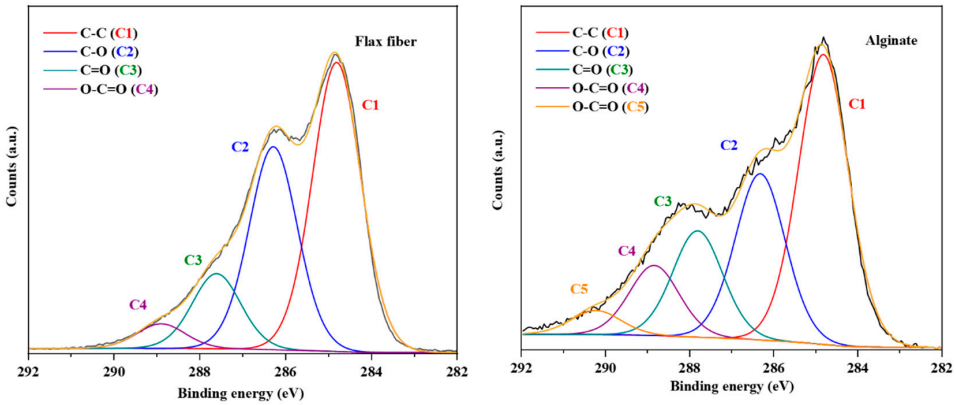

Figure 6. XPS C1s spectra of untreated flax fiber and sodium alginate samples.

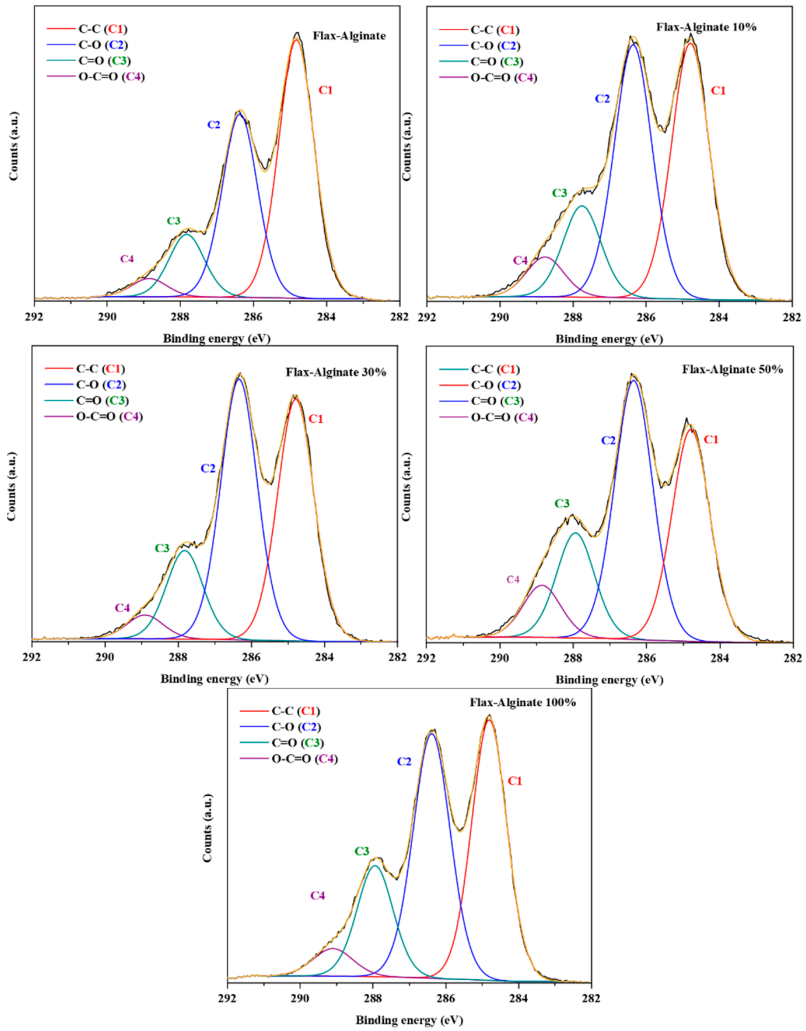

Figure 7. Surface chemical modifications of flax–alginate samples evidenced via XPS following plasma treatment.

3.4. SEM

Figure 8 presents a thorough examination of flax–alginate samples under various plasma treatment conditions, utilizing both digital photographs and SEM images at different magnifications. First, the digital image of a flax–alginate sample shows a close-up texture related to a mass of fine fibers, likely composed of short flax fibers with no distinct pattern or weave. The SEM image of this sample at 50 µm magnification clearly displays the continuous film of sodium alginate around fibers that act as a binder in maintaining structural integrity within the mat. For DCs of 10% and 30%, the digital photographs display no noticeable changes in appearance, highlighting the material's stability after modification. In contrast, the SEM images at 50 µm reveal subtle transformations. At a 10% DC, the alginate binder showed signs of minor wear, with visible wear in some areas. Moreover, by the 30% duty cycle, the wear became more pronounced, with many more spots showing signs of degradation. This increased wear was not due to a change in the intensity of the plasma treatment, as both the voltage and frequency remained constant. Instead, it highlighted the material's changing response to a longer exposure time to the plasma, as the 30% duty cycle effectively increased the duration of each discharge cycle. Despite these changes at the micro-level, the fibers remained interconnected, preserving the overall structural integrity of the material. At a DC of 50%, visible signs of degradation began to appear on the digital images, including holes and gaps, indicating a reduced effectiveness of the alginate in binding the material together. The SEM images provided further confirmation, revealing a significant degradation in the alginate film. This level of modification aligns with the observed increase in ΔT, as reported in the OES section. At this stage, one should consider that an intensified interaction between the filaments in the discharge and the surface that underwent a longer time of treatment are likely responsible for these strong morphological modifications. This finding is crucial as it links with the study reported by Borcia et al. [48]. In their study on plasma-treated polymers like PET and nylon fabrics, they highlighted that filamentary discharge could result in highly localized and intense fabric degradation. At a 100% DC, the material highlights extensive degradation on the digital images, suggesting a significant structural transformation. The SEM images lend further support to these findings, showcasing an almost absence of the alginate film and greater morphological modification of the fibers. This level of degradation corresponds to an extremely high interaction energy, signifying a critical change in the material's response to the plasma treatment. The SEM analysis from the study by Doaa. M. El-Zeer et al. [49] on wool fibers treated with high power plasma showed similarities with our observations. In their work, the authors reported the presence of microcracks and microholes in the material due to a strong oxidation process. While the etching process in their study led to a softer feel of the fibers, it also caused damage to the textile, especially at high power levels. Therefore, this high level of degradation at a 100% DC, mirrored in findings from other studies on high-power plasma-treated fibers, led to the decision to avoid these conditions for composite production, as they were deemed detrimental to their integrity.

3.5. DSC

The thermal behavior of the short flax fiber composites treated with plasma-enhanced alginate was extensively analyzed using differential scanning calorimetry (DSC), and the results are depicted in Figures 9 and 10. Figure 9 illustrates the DSC curve during the first heating cycle of the composite material. During the first heating cycle, in the range of 50–70 °C, a distinct endothermic reaction characterized the glass transition temperature (T_g), which signifies the material's transition from a glassy to a rubbery state. The T_g provides insight into the flexibility and service temperature of the composite materials. For the samples treated at 10% and 30% duty cycles (DCs), the T_g displayed marginal deviations from the untreated composites, suggesting that lower plasma intensities do not significantly disrupt the polymer matrix. However, at a 50% DC, the upward shift in T_g

indicates an increase in chain mobility, possibly due to the plasma treatment facilitating better polymer–fiber interactions, as also inferred from SEM analyses.

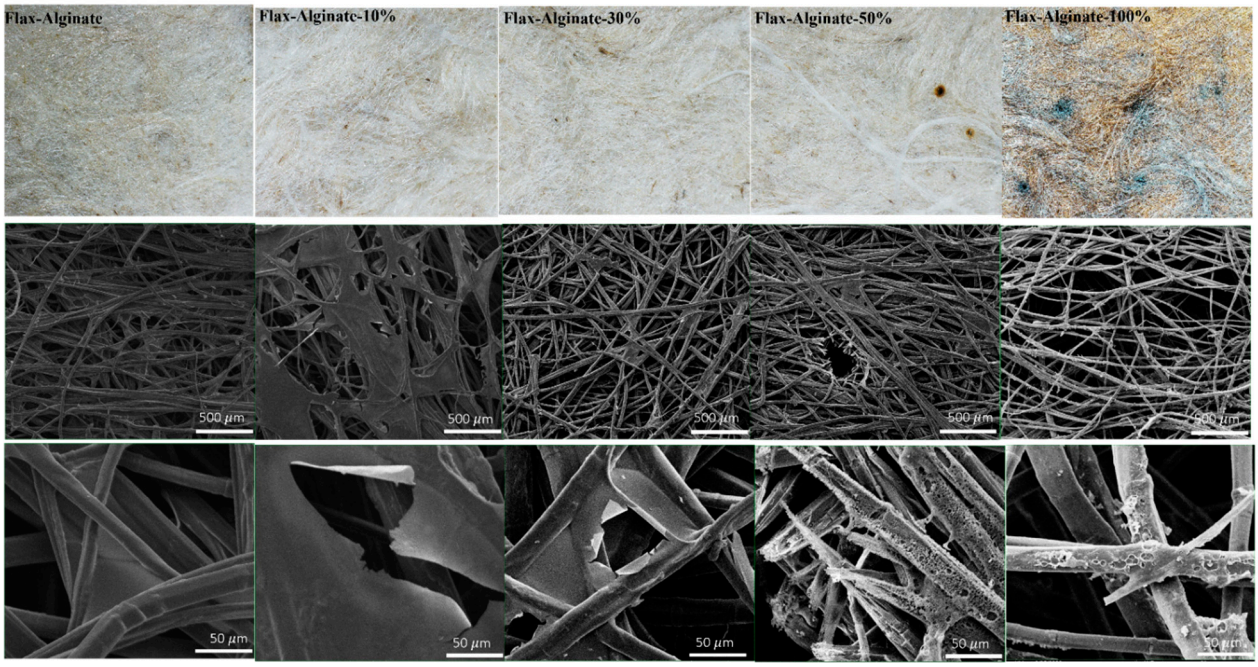

Figure 8. Digital and SEM visualizations of flax–alginate samples at varied plasma duty cycles.

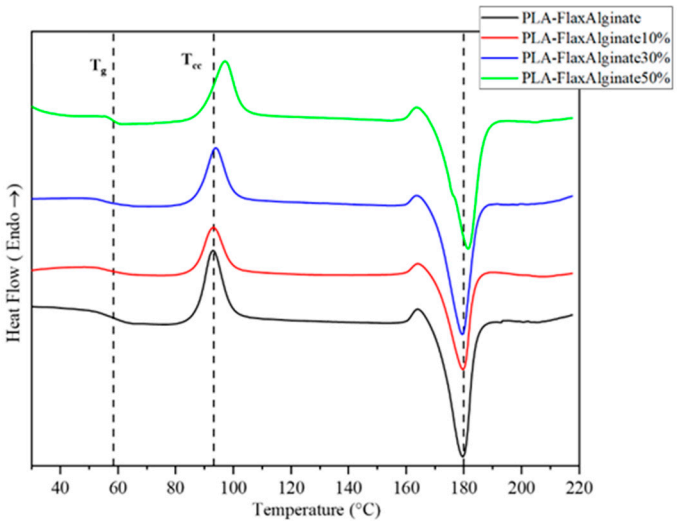

Figure 9. DSC thermogram during first heating of PLA–flax–alginate composites.

The crystallization temperature (T_{cc}) and melting temperature (T_m) offer a window into the thermal stability and crystalline nature of the composites. Samples maintained at 10% and 30% DCs mirrored the thermal behavior of untreated fibers, indicating the preservation of native crystallinity. In contrast, for the sample treated at a 50% DC, the T_{cc} and T_m occur at higher temperatures. This suggests a need for increased energy to initiate crystallization. The reason behind this is the strengthened interface between the fiber and the matrix, which results in a firmer attachment of the polymer chains to the fibers, consequently reducing their mobility and thereby delaying the crystallization process [18,50].

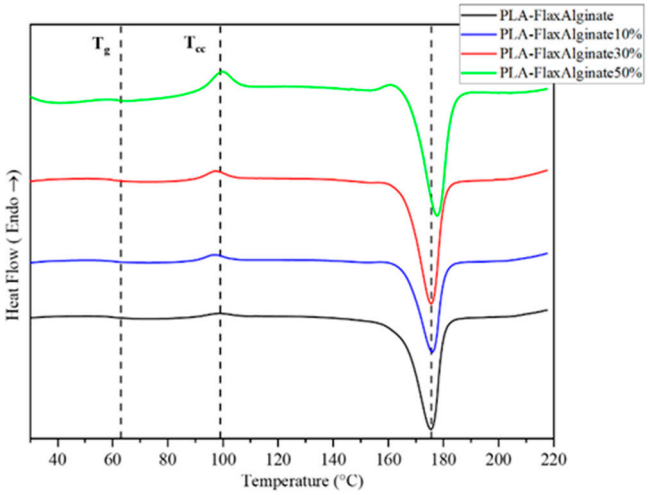

Figure 10. DSC thermogram during second heating of PLA–flax–alginate composites.

A subsequent analysis during the second heating cycle provided validation of these findings, showcasing the reproducibility and stability of the thermal properties post treatment. This cycle is crucial as it eliminates the thermal history of the first heating and showcases the inherent material behavior more accurately. The untreated and low-intensity treated samples (10% and 30% DCs) retained their thermal integrity. However, the 50% DC samples showed an increased melting temperature, which makes them suitable for higher-temperature applications.

Table 3 reveals how plasma treatment modulates the PLA–flax–alginate composites' crystallinity and heat of fusion. The data show a decrease in both properties at a 10% DC, implying an increase in amorphous regions, which could enhance material toughness. At a 30% DC, values approximate those of untreated composites, suggesting a plasma treatment threshold that maintains the material's inherent structure. Notably, at a 50% DC, increases in crystallinity and heat of fusion indicate a potential for greater mechanical strength and thermal stability, which are desirable in demanding applications.

Table 3. Crystallinity of PLA–flax–alginate composites post plasma treatment.

Sample	Heat of Fusion (J/g)	Crystallinity (%)
PLA–Flax–Alginate	0.0523	0.0563
PLA–Flax–Alginate 10%	0.0360	0.0387
PLA–Flax–Alginate 30%	0.0519	0.0558
PLA–Flax–Alginate 50%	0.0590	0.0634

3.6. DMA

DMA was employed to evaluate the effects of plasma treatment on the PLA–flax–alginate composites, with a particular focus on understanding changes in storage and loss modulus. Figures 11 and 12 depict variations in the storage modulus and loss modulus with temperature for different plasma treatment conditions, offering a visual comprehension of the DMA data.

The integration of modified fibers into PLA composites, shown in Figure 11, resulted in a noticeable enhancement of stiffness across all measured temperatures. In particular, a visible decrease in stiffness is observed in the PLA curve from 50 °C to 80 °C. This phase likely denotes the glass transition phase, marked by a shift from a stiffer to a more flexible state. The addition of alginate-modified flax fibers has led to improvement in the storage modulus, which is indicative of strengthened mechanical properties. The flax fibers reveal additional rigidity, while the alginate modification presumably improves the bond between the fibers and the PLA matrix, optimizing stress distribution across the material [51].

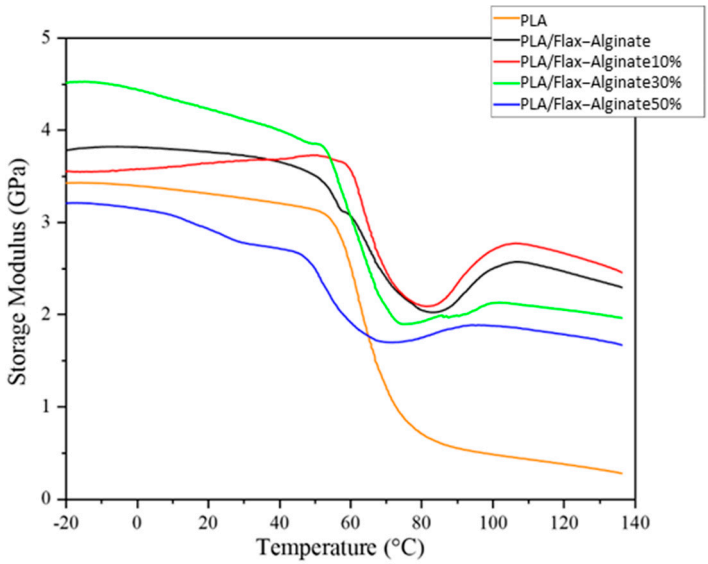

Figure 11. DMA of PLA–flax–alginate composites: storage modulus variations across different plasma treatment intensities.

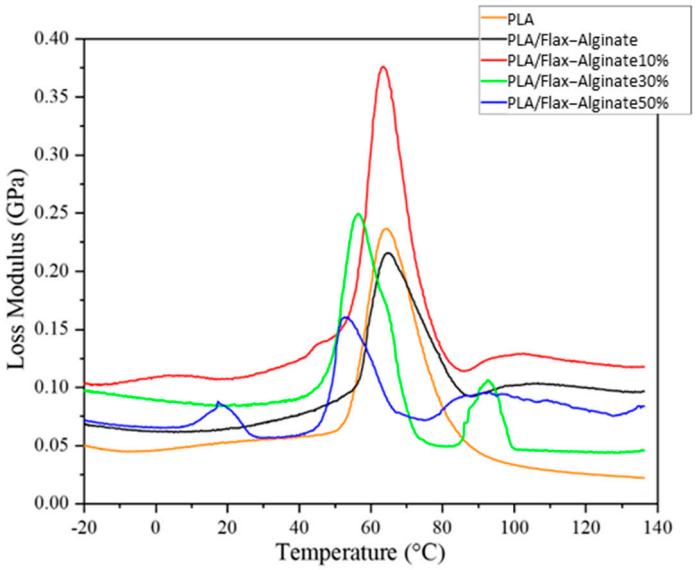

Figure 12. DMA of PLA–flax–alginate composites: loss modulus variations across different plasma treatment intensities.

Samples subjected to low-intensity plasma treatment, especially at 10% and 30% duty cycles, consistently exhibited increased stiffness. The sample treated with 30% plasma showed the highest storage modulus. This suggests that this level of plasma treatment effectively introduced polar groups onto the fibers' surfaces, as confirmed through FTIR data, thereby improving their adhesion with the PLA matrix. This enhanced adhesion optimizes the stress distribution within the composite, resulting in increased stiffness and mechanical resilience, without causing significant fiber degradation. In contrast, the PLA–flax–alginate 50% sample revealed a decrease in storage modulus, hinting at potential adverse effects of intense plasma treatment on the flax fibers and their interactions with the PLA matrix.

As the temperature exceeded 80 °C, a discernible decline in the storage modulus of the PLA was observed, which is indicative of a decrease in mechanical stiffness. Conversely, the composite samples demonstrated a notable recovery in storage modulus at temperatures beyond this threshold. This recovery can be potentially attributed to the process of material

recrystallization, which, consequentially, may enhance the mechanical properties of the composites [23].

The loss modulus, a parameter indicative of a material's ability to dissipate energy as heat, reveals intriguing patterns across various composite formulations. In the case of pure PLA, the loss modulus exhibits a pronounced peak within the temperature range of 50 °C to 80 °C. This peak corresponds to the material's phase transition and is indicative of an optimum in the material's damping characteristics.

A noticeable yet subtle shift in the peak of the loss modulus toward lower temperatures was observed in the PLA–flax–alginate composites, specifically for those with 30% and 50% compositions, when compared to the baseline of untreated PLA and the PLA–flax-alginate composite. This shift is more marked in the sample with a 50% DC, which can be ascribed to changes in the fiber–matrix interactions and the overall structure of the composite induced by plasma treatment. Such alterations explain the profound influence of plasma treatments on the viscoelastic properties of the material.

In the PLA–flax-alginate 50% sample, a discernible peak within the 10–30 °C range on the loss modulus curve is associated with β-relaxation. This relaxation indicates localized motions in polymer chains at temperatures below the T_g and arises from the side groups or shorter chain segments moving independently **[52]**. This behavior is likely due to the interactions between the PLA matrix and the modified flax fibers following a 50% DC plasma treatment. Such treatment induces subtle yet critical changes within the material, influencing its mechanical response under dynamic conditions [53].

In contrast, the PLA–flax–alginate 30% sample exhibits a significant peak in the loss modulus curve within the 80–100 °C range, which may be indicative of α-relaxation. This relaxation process, characterized by an increase in segmental mobility within the polymer, is typically the most pronounced relaxation event and correlates closely with the T_g of the material. The observed shift in the transition of viscoelastic properties to a higher temperature range, consequent to the 30% plasma treatment, implies an enhancement of the material's stability. It also suggests that the composite's performance is maintained over a broader temperature range, indicative of its potential for applications requiring thermal resilience.

4. Conclusions

In this study, a comprehensive evaluation was conducted on the impact of plasma-enhanced alginate pre-treatment on short flax fibers, marking a significant advancement in the domain of sustainable composite materials. The effects of varying plasma duty cycles (DCs) on the mechanical, chemical, and microstructural properties of the samples were meticulously analyzed.

The research began with an OES analysis of flax fibers during nitrogen discharge treatment. It was observed that the intensity of CN emissions significantly increased over time, especially at higher DCs. Notable rises in dielectric temperature was also depicted with the DCs. Specifically, temperature rises of 34 °C and 64 °C were observed for DCs of 50% and 100%, respectively. Conversely, NO emissions did not exhibit a clear time trend but showed a decrease in intensity with increasing DC. This was accompanied by a reduction in vibrational temperature at higher DCs, suggesting that changes in the discharge chemistry can potentially be linked to the fiber degradation.

Moving to the ATR-FTIR study, chemical modifications were identified, particularly at the 30% plasma treatment level. The emergence of a peak at 1713 cm^{-1} was indicative of oxidation and the introduction of polar carbonyl groups, suggesting an enhancement in the material's surface properties and adhesion potential.

Through XPS analysis, it was revealed that plasma treatment alters the surface chemistries of the samples. This was evidenced by an increase in oxygen content and a decrease in carbon levels, with a notable rise in the O/C ratio. Following plasma treatments at 10%, 30%, and 50% duty cycles, the O/C ratio increased to 0.5257, 0.5234, and 0.6503, respectively. These changes suggest an enhancement of oxygen-containing functional groups

on the surface. Additionally, the appearance and intensification of peaks corresponding to C=O bonds in the C1s spectra after plasma treatment indicate the formation of or increase in carbonyl groups, aligning with the FTIR analysis findings.

SEM imaging provided a visual perspective on the material's structural changes. It was evident that increasing plasma intensity progressively degraded the material's structure. At lower duty cycles (10% and 30%), subtle surface modifications occurred without compromising the overall material integrity, as indicated by minor wear in the SEM images. However, at higher duty cycles (50% and 100%), significant degradation was observed, with the 50% DC showing holes and gaps and the 100% DC leading to a near-complete breakdown of the alginate film and the exposure of the fibers. This extensive wear at the highest DC suggests that such intense plasma treatment conditions are detrimental to the composite's structural integrity, rendering them unsuitable for composite production.

Finally, the DSC analysis highlighted that plasma treatment, particularly at a 50% duty cycle, changed the thermal properties of the composites. Increases in both glass transition and crystallization temperatures were observed, suggesting improved polymer–fiber interaction and increased chain mobility. Moreover, the DMA revealed that the 30% plasma treatment significantly enhanced the mechanical properties of the composite. This treatment level optimally increased the storage modulus, indicating improved stiffness and mechanical resilience, as evidenced by the substantial increase in the storage modulus from 3.4 GPa for PLA to 4.5 GPa for the samples treated at a DC of 30%, while also shifting the peak in the loss modulus to higher temperatures. This shift suggests enhanced thermal stability and a broader operational temperature range, making the 30% plasma-treated composite particularly suitable for applications requiring both mechanical strength and thermal resilience.

Author Contributions: Conceptualization, G.M., J.P., M.R., G.L., S.E. and F.M.; Methodology, G.M., J.P., S.E. and F.M.; Validation, G.M., J.P. and S.E.; Formal analysis, G.M., J.P. and S.E.; Investigation, G.M., J.P., A.D., S.E. and P.Y.V.; Writing—original draft, G.M.; Writing—review & editing, G.M., J.P., M.R., G.L., S.E., F.M. and P.Y.V.; Visualization, G.M., J.P., M.R., G.L., S.E. and F.M.; Supervision, J.P., M.R., G.L., S.E. and F.M.; Project administration, S.E.; Funding acquisition, M.R., G.L., S.E. and F.M. All authors have read and agreed to the published version of the manuscript.

Funding: This research received no external funding.

Data Availability Statement: Dataset available on request from the authors.

Acknowledgments: The authors acknowledge the Center for High Performance Polymer and Composite Systems (CREPEC), Quebec Centre for Advanced Materials (CQMF), and Canada Research Chair in Polymer Eco-Composites for financial support.

Conflicts of Interest: The authors declare no conflict of interest.

References

1. Bernaoui, A.; Lebrun, G.; Ruiz, E. High performance natural fiber composites from mat and UD flax reinforcements backed with a mat Binder: A study of mat fiber surface fibrillation. *Compos. Part A Appl. Sci. Manuf.* **2022**, *160*, 107064. [CrossRef]
2. Natural Fiber Composites Market by Type, Resin Type, Manufacturing Process, End-Use Industry, Region—Global Forecast to 2028. June 2023. Available online: https://www.marketsandmarkets.com/Market-Reports/natural-fiber-composites-market-90779629.html?gclid=CjwKCAjw38SoBhB6EiwA8EQVLonY01ntUZNzlcNJb3aEjuveyaz-wef5uYun9AWe9nNF-div8PEeTRoCmckQAvD_BwE (accessed on 31 June 2023).
3. Plakantonaki, S.; Kiskira, K.; Zacharopoulos, N.; Chronis, I.; Coelho, F.; Togiani, A.; Kalkanis, K.; Priniotakis, G. A Review of Sustainability Standards and Ecolabeling in the Textile Industry. *Sustainability* **2023**, *15*, 11589. [CrossRef]
4. Sigaard, A.S.; Laitala, K. Natural and sustainable? Consumers' textile fiber preferences. *Fibers* **2023**, *11*, 12. [CrossRef]
5. Nassiopoulos, E.; Njuguna, J. Thermo-mechanical performance of poly (lactic acid)/flax fibre-reinforced biocomposites. *Mater. Des.* **2015**, *66*, 473–485. [CrossRef]
6. Sanivada, U.K.; Mármol, G.; Brito, F.; Fangueiro, R. PLA composites reinforced with flax and jute fibers—A review of recent trends, processing parameters and mechanical properties. *Polymers* **2020**, *12*, 2373. [CrossRef] [PubMed]
7. Muñoz, E.; García-Manrique, J.A. Water absorption behaviour and its effect on the mechanical properties of flax fibre reinforced bioepoxy composites. *Int. J. Polym. Sci.* **2015**, *2015*, 390275. [CrossRef]

8. Bayart, M.; Gauvin, F.; Foruzanmehr, M.R.; Elkoun, S.; Robert, M. Mechanical and moisture absorption characterization of PLA composites reinforced with nano-coated flax fibers. *Fibers Polym.* **2017**, *18*, 1288–1295. [CrossRef]
9. Wang, W.; Lowe, A.; Kalyanasundaram, S. Effect of chemical treatments on flax fibre reinforced polypropylene composites on tensile and dome forming behaviour. *Int. J. Mol. Sci.* **2015**, *16*, 6202–6216. [CrossRef]
10. Bozaci, E.; Sever, K.; Sarikanat, M.; Seki, Y.; Demir, A.; Ozdogan, E.; Tavman, I. Effects of the atmospheric plasma treatments on surface and mechanical properties of flax fiber and adhesion between fiber–matrix for composite materials. *Compos. Part B Eng.* **2013**, *45*, 565–572. [CrossRef]
11. Lee, S.G.; Choi, S.S.; Park, W.H.; Cho, D. Characterization of surface modified flax fibers and their biocomposites with PHB. *Macromol. Symp.* **2003**, *197*, 089–100. [CrossRef]
12. Ishak, A.; Sonnier, R.; Otazaghine, B.; Longuet, C. Silazanes, a novel flax fibers functionalization: Effect on silicone-based composites. *Compos. Part A Appl. Sci. Manuf.* **2023**, *166*, 107382. [CrossRef]
13. Koohestani, B.; Darban, A.; Mokhtari, P.; Yilmaz, E.; Darezereshki, E. Comparison of different natural fiber treatments: A literature review. *Int. J. Environ. Sci. Technol.* **2019**, *16*, 629–642. [CrossRef]
14. Babaei, S.; Profili, J.; Asadollahi, S.; Sarkassian, A.; Dorris, A.; Beck, S.; Stafford, L. Analysis of transport phenomena during plasma deposition of hydrophobic coatings on porous cellulosic substrates in plane-to-plane dielectric barrier discharges at atmospheric pressure. *Plasma Process. Polym.* **2020**, *17*, 2000091. [CrossRef]
15. Levasseur, O.; Profili, J.; Gangwar, R.; Naudé, N.; Clergereaux, R.; Gherardi, N.; Stafford, L. Experimental and modelling study of organization phenomena in dielectric barrier discharges with structurally inhomogeneous wood substrates. *Plasma Sources Sci. Technol.* **2014**, *23*, 054006. [CrossRef]
16. Meunier, L.F.; Profili, J.; Babaei, S.; Asadollahi, S.; Sarkissian, A.; Dorris, A.; Beck, S.; Naudé, N.; Stafford, L. Modification of microfibrillated cellulosic foams in a dielectric barrier discharge at atmospheric pressure. *Plasma Process. Polym.* **2021**, *18*, 2000158. [CrossRef]
17. Gupta, R.K.; Guha, P.; Srivastav, P.P. Effect of high voltage dielectric barrier discharge (DBD) atmospheric cold plasma treatment on physicochemical and functional properties of taro (*Colocasia esculenta*) starch. *Int. J. Biol. Macromol.* **2023**, *253*, 126772. [CrossRef]
18. Moradkhani, G.; Profili, J.; Robert, M.; Laroche, G.; Elkoun, S. Effects of Wet and Dry Treatments on Surface Functional Groups and Mechanical Properties of Flax Fiber Composites. *Coatings* **2023**, *13*, 1036. [CrossRef]
19. Pizzi, A.; Scharfetter, H.; Kes, E.W. Adhesives and techniques open new possibilities for the wood processing industry. I. Experience with tannin based adhesives. *Holz Als Roh- Und Werkst.* **1981**, *39*, 85–89. [CrossRef]
20. Ghaffar, S.H.; Fan, M. Lignin in straw and its applications as an adhesive. *Int. J. Adhes. Adhes.* **2014**, *48*, 92–101. [CrossRef]
21. Nicollin, A.; Kueny, R.; Toniazzo, L.; Pizzi, A. High density biocomposite from natural fibers and tannin resin. *J. Adhes. Sci. Technol.* **2012**, *26*, 1537–1545. [CrossRef]
22. Pizzi, A.; Kueny, R.; Lecoanet, F.; Massetau, B.; Carpentier, D.; Krebs, A.; Loiseau, F.; Molina, S.; Ragoubi, M. High resin content natural matrix–natural fibre biocomposites. *Ind. Crops Prod.* **2009**, *30*, 235–240. [CrossRef]
23. Bayart, M.; Adjallé, K.; Diop, A.; Ovlaque, P.; Barnabé, S.; Robert, M.; Elkoun, S. PLA/flax fiber bio-composites: Effect of polyphenol-based surface treatment on interfacial adhesion and durability. *Compos. Interfaces* **2021**, *28*, 287–308. [CrossRef]
24. El-Gaayda, J.; Titchou, F.E.; Oukhrib, R.; Yap, P.-S.; Liu, T.; Hamdani, M.; Akbour, R.A. Natural flocculants for the treatment of wastewaters containing dyes or heavy metals: A state-of-the-art review. *J. Environ. Chem. Eng.* **2021**, *9*, 106060. [CrossRef]
25. Eslami, Z.; Elkoun, S.; Robert, M.; Adjallé, K. A Review of the Effect of Plasticizers on the Physical and Mechanical Properties of Alginate-Based Films. *Molecules* **2023**, *28*, 6637. [CrossRef] [PubMed]
26. Lacoste, C.; El Hage, R.; Bergeret, A.; Corn, S.; Lacroix, P. Sodium alginate adhesives as binders in wood fibers/textile waste fibers biocomposites for building insulation. *Carbohydr. Polym.* **2018**, *184*, 1–8. [CrossRef]
27. Raus, R.A.; Nawawi, W.M.F.W.; Nasaruddin, R.R. Alginate and alginate composites for biomedical applications. *Asian J. Pharm. Sci.* **2021**, *16*, 280–306. [CrossRef]
28. John, M.J. Biobased alginate treatments on flax fibre reinforced PLA and PHBV composites. *Curr. Res. Green Sustain. Chem.* **2022**, *5*, 100319. [CrossRef]
29. Machala, Z.; Janda, M.; Hensel, K.; Jedlovský, I.; Leštinská, L.; Foltin, V.; Martišovitš, V.; Morvova, M. Emission spectroscopy of atmospheric pressure plasmas for bio-medical and environmental applications. *J. Mol. Spectrosc.* **2007**, *243*, 194–201. [CrossRef]
30. Tyl, C.; Lin, X.; Bouzidi, M.; Dap, S.; Caquineau, H.; Ségur, P.; Gherardi, N.; Naudé, N. Investigation of memory effect in atmospheric pressure dielectric barrier discharge in nitrogen with small oxygen or nitric oxide addition. *J. Phys. D Appl. Phys.* **2018**, *51*, 354001. [CrossRef]
31. Gherardi, N.; Gouda, G.; Gat, E.; Ricard, A.; Massines, F. Transition from glow silent discharge to micro-discharges in nitrogen gas. *Plasma Sources Sci. Technol.* **2000**, *9*, 340. [CrossRef]
32. Massines, F.; Segur, P.; Gherardi, N.; Khamphan, C.; Ricard, A. Physics and chemistry in a glow dielectric barrier discharge at atmospheric pressure: Diagnostics and modelling. *Surf. Coat. Technol.* **2003**, *174*, 8–14. [CrossRef]
33. Masoud, N.; Martus, K.; Figus, M.; Becker, K. Rotational and vibrational temperature measurements in a high-pressure cylindrical dielectric barrier discharge (C-DBD). *Contrib. Plasma Phys.* **2005**, *45*, 32–39. [CrossRef]
34. Lawrie, G.; Keen, I.; Drew, B.; Chandler-Temple, A.; Rintoul, L.; Fredericks, P.; Grøndahl, L. Interactions between alginate and chitosan biopolymers characterized using FTIR and XPS. *Biomacromolecules* **2007**, *8*, 2533–2541. [CrossRef] [PubMed]

35. Aprilliza, M. Characterization and properties of sodium alginate from brown algae used as an ecofriendly superabsorbent. In Proceedings of the International Symposium on Current Progress in Functional Materials, Bali, Indonesia, 26–27 July 2016; IOP Conference Series: Materials Science and Engineering. IOP Publishing: Bristol, UK, 2016; p. 012019.
36. Badita, C.; Aranghel, D.; Burducea, C.; Mereuta, P. Characterization of sodium alginate based films. *Rom. J. Phys* **2020**, *65*, 1–8.
37. Ferreira, D.P.; Cruz, J.; Fangueiro, R. Surface modification of natural fibers in polymer composites. In *Green Composites for Automotive Applications*; Elsevier: Amsterdam, The Netherlands, 2019; pp. 3–41.
38. Kramar, A.D.; Obradović, B.M.; Schiehser, S.; Potthast, A.; Kuraica, M.M.; Kostić, M.M. Enhanced antimicrobial activity of atmospheric pressure plasma treated and aged cotton fibers. *J. Nat. Fibers* **2022**, *19*, 7391–7405. [CrossRef]
39. Akindoyo, J.O.; Beg, M.D.; Ghazali, S.; Heim, H.P.; Feldmann, M. Effects of surface modification on dispersion, mechanical, thermal and dynamic mechanical properties of injection molded PLA-hydroxyapatite composites. *Compos. Part A Appl. Sci. Manuf.* **2017**, *103*, 96–105. [CrossRef]
40. Gholami, M.; Ahmadi, M.S.; Tavanaie, M.A.; Khajeh Mehrizi, M. Effect of oxygen plasma treatment on tensile strength of date palm fibers and their interfacial adhesion with epoxy matrix. *Sci. Eng. Compos. Mater.* **2018**, *25*, 993–1001. [CrossRef]
41. Rasch, R.; Stricher, A.; Truss, R.W. Energy filtered low voltage "in lens detector" SEM and XPS of natural fiber surfaces. *J. Appl. Polym. Sci.* **2014**, *131*, 39572. [CrossRef]
42. Mukherjee, A.; Okolie, J.A.; Niu, C.; Dalai, A.K. Experimental and modeling studies of torrefaction of spent coffee grounds and coffee husk: Effects on surface chemistry and carbon dioxide capture performance. *ACS Omega* **2021**, *7*, 638–653. [CrossRef]
43. Awada, H.; Elchinger, P.-H.; Faugeras, P.-A.; Zerrouki, C.; Montplaisir, D.; Brouillette, F.; Zerrouki, R. Chemical modification of kraft cellulose fibres: Influence of pretreatment on paper properties. *BioResources* **2015**, *10*, 2044–2056. [CrossRef]
44. Liu, M.; Meng, Q.; Niu, C.; Wang, Y.; Zhou, G.; Xu, C.; Liu, Y. Preparation and characterization of modified dual network dust suppression gel based on sodium alginate and soluble starch. *Environ. Sci. Pollut. Res.* **2022**, *29*, 69771–69784. [CrossRef]
45. Tam, S.K.; Dusseault, J.; Polizu, S.; Ménard, M.; Hallé, J.-P. Physicochemical model of alginate–poly-l-lysine microcapsules defined at the micrometric/nanometric scale using ATR-FTIR, XPS, and ToF-SIMS. *Biomaterials* **2005**, *26*, 6950–6961. [CrossRef] [PubMed]
46. Milaniak, N.; Laroche, G.; Massines, F. Fourier-transform infrared spectroscopy of ethyl lactate decomposition and thin-film coating in a filamentary and a glow dielectric barrier discharge. *Plasma Process. Polym.* **2021**, *18*, 2000248. [CrossRef]
47. Zhuoda, J. Effects of plasma treatment of carbon fibers on interfacial properties of BMI resin composites. *Surf. Interface Anal.* **2019**, *51*, 458–464. [CrossRef]
48. Borcia, G.; Anderson, C.; Brown, N. Surface treatment of natural and synthetic textiles using a dielectric barrier discharge. *Surf. Coat. Technol.* **2006**, *201*, 3074–3081. [CrossRef]
49. El-Zeer, D.M.; Salem, A.A.; Rashed, U.M.; Abd Elbaset, T.A.; Ghalab, S. A comparative study between the filamentary and glow modes of DBD plasma in the treatment of wool fibers. *Int. J. Eng. Res. Appl.* **2014**, *4*, 1.
50. Foruzanmehr, M.; Vuillaume, P.Y.; Elkoun, S.; Robert, M. Physical and mechanical properties of PLA composites reinforced by TiO2 grafted flax fibers. *Mater. Des.* **2016**, *106*, 295–304. [CrossRef]
51. Gao, C.; Guo, J.; Xie, H. The effect of alginate on the mechanical, thermal, and rheological properties of nano calcium carbonate-filled polylactic acid composites. *Polym. Eng. Sci.* **2019**, *59*, 1882–1888. [CrossRef]
52. McCrum, N.G.; Buckley, C.P.; Bucknall, C.B. *Principles of Polymer Engineering*; Oxford University Press: Oxford, UK, 1997.
53. Hearle, J.W.; Morton, W.E. *Physical Properties of Textile Fibres*; Elsevier: Amsterdam, The Netherlands, 2008.